ADVANCED MATERIALS

www.advmat.de

Morphology Tunable Hybrid Carbon Nanosheets with Solvatochromism

Yuri Choi, Sunghu Kim, Yeongkyu Choi, Jaeeun Song, Tae-Hyuk Kwon, Oh-Hoon Kwon, and Byeong-Su Kim**

The tunable photoluminescence of carbon-based nanomaterials has received much attention for a wide range of applications. Herein, a unique, broad-solvatochromic hybrid carbon nanosheet (CNS) synthesized through the hydrothermal carbonization of molecular precursors exploiting graphene oxide as a template is reported, resulting in the formation of clusters of carbon nanorings on the surface of graphene-oxide nanosheets. Under UV and visible-light excitation, the hybrid CNS exhibits tunable emission spanning the wide range of colors in a series of solvents with different polarities. This interesting spectroscopic behavior is found to originate from hydrogen-bonding interactions between CNS and solvents, which eventually induce the morphological transition of CNS from 2D sheets to 3D crumpled morphologies, affecting the lifetimes of emissive states. This novel soft carbon nanostructure may open up a new possibility in tailoring the photophysical properties of carbon nanomaterials.

Photoluminescent carbon nanomaterials have attracted considerable interest owing to their unique optical properties and photostability, which are useful for optoelectronic devices, biological labels, and sensors.[1] To date, different mechanistic frameworks have been proposed to elucidate the origin of the photoluminescence (PL) of carbon nanomaterials depending on their crystal structure, dimension, and chemical functionalization.[2] In many cases, however, the PL of carbon nanomaterials has a narrow color range, mostly with blue emission of relatively low quantum yield (QY), which potentially limits their practical applications.[3] To address these critical challenges, several approaches have been explored for improving the PL behaviors of carbon nanomaterials, including synthetic control using various precursors, surface passivation, heteroatom doping, chemical reduction, and postsynthetic approaches such as chromatographic separation.[4]

Dr. Y. Choi, S. Kim, Y. Choi, J. Song, Prof. T.-H. Kwon, Prof. O.-H. Kwon, Prof. B.-S. Kim
Department of Chemistry
Ulsan National Institute of Science and Technology (UNIST)
Ulsan 44919, Korea
E-mail: ohkwon@unist.ac.kr; bskim19@unist.ac.kr
Prof. O.-H. Kwon
Center for Soft and Living Matter
Institute for Basic Science (IBS)
Ulsan 44919, Korea

DOI: 10.1002/adma.201701075

Besides the aforementioned synthetic approaches, medium environment, such as solvent polarity, can also affect the PL spectra of luminophores, which is called solvatochromism. As often found in organic dyes, the electronic-transition energy can change through solute–solvent interaction, resulting in the shift of absorption and PL spectra, but to a limited extent.[5] Recently, carbon nanomaterials such as carbon nanotubes, graphene oxide (GO), and carbon dots (CDs) have also been reported to exhibit tunable PL on account of the preferential interaction with solvent molecules or the presence of different surface trap states with varying solvent polarity.[6] Despite significant progress in the development of carbon nanomaterials showing solvent-dependent PL, only few examples of the tunability covering the wide range of colors has been reported.[7]

Toward this end, novel types of hybrid carbon nanostructures that possess unique properties and structures have been introduced.[8] In particular, GO, an oxidized analogue of graphene, has been proposed for the modulation of the molecular configuration of carbon nanomaterials because of its surface functional groups together with its high specific surface area.[9] For example, GO can change the spherical morphology of carbonized glucose to a 2D structure under hydrothermal carbonization.[10]

Herein, we report a unique design and synthesis of hybrid carbon nanosheets (CNSs), which show strong solvatochromic behavior with wide color tunability ranging from blue to orange and even to white in various solvents. The hybrid CNS hosts clusters of carbon nanorings on the surface of GO nanosheets as the product of the hydrothermal reaction of small molecular precursors in the presence of GO nanosheets. Unlike the typical formation of spherical CDs in the absence of a GO template, the molecular precursors turned into concentric carbon nanorings with the aid of the GO template during carbonization. The prepared CNS displayed highly tunable emission covering the visible ranges depending on the solvent. A detailed mechanistic framework was carefully developed through a series of spectroscopic analyses, including UV–vis, PL, Fourier-transform infrared spectroscopy (FT-IR), X-ray photoelectron spectroscopy (XPS), and time-resolved electronic spectroscopy. Toward the realization of wide emission of hybrid carbon nanomaterials, this study revealed the origin of solvatochromic PL, which is accompanied by a morphological transition of soft

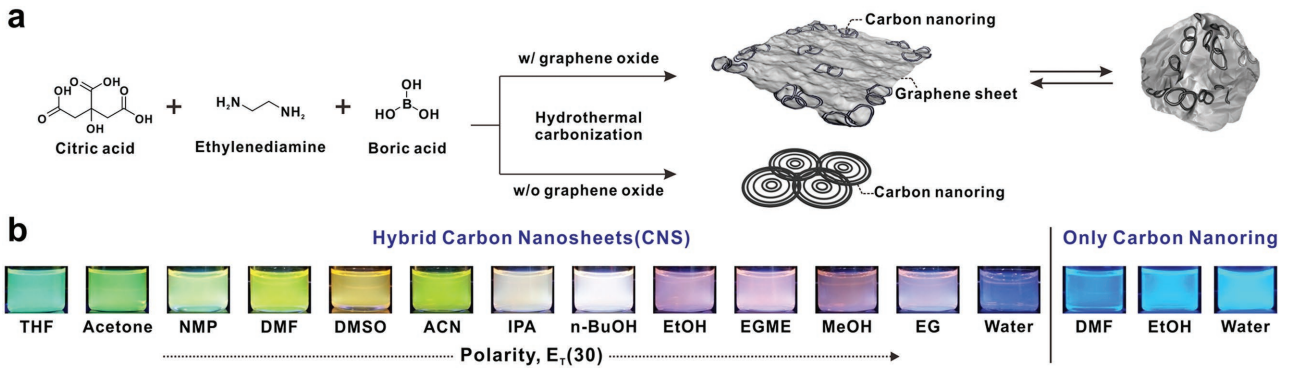

Figure 1. Synthesis and optical properties of hybrid carbon nanosheets (CNSs). a) Schematic representation of the synthetic procedure of CNS. b) Optical images of CNS suspensions in different solvents (concentration of 0.10 mg mL^{-1}) when excited at 365 nm. Control set of carbon nanorings without solvatochromism in their representative solvents are shown for comparison. Solvents are listed from low- to high-polarity solvents based on $E_T(30)$ values. See the text for acronyms of the solvents.

hybrid CNS depending on the solvent. We found that the different degrees of the exposure of surface functional groups to the solvent and the solute–solvent hydrogen (H)-bonding interactions are responsible for the morphological change, and these factors affect the nonradiative relaxation of the photoexcited surface functional groups causing the steady-state spectral modulation of PL.

CNS was initially prepared through the hydrothermal decomposition of small organic molecules such as citric acid, boric acid, and ethylenediamine in the presence of GO nanosheets (see **Figure 1**a and the Experimental Section for details). The composition of the simple organic molecules was based on our previous approach in the synthesis of highly photoluminescent boron- and nitrogen-doped CDs.[11] With the assistance of the graphitic framework of a GO nanosheet used in the synthesis, the hydrothermal decomposition preferentially occurred on the surface of the GO nanosheet. Other carbonaceous residues were successfully removed through extensive rinsing and precipitation steps using a mixture of chloroform and ethanol. After these purification steps, the final product isolated from the supernatant consisted of graphene-like sheets hosting clusters of anchored nanorings (Figure 1a). When recovered and redissolved in different solvents of varying polarity, including tetrahydrofuran (THF), acetone, *N*-methyl-2-pyrrolidone (NMP), dimethylformamide (DMF), dimethyl sulfoxide (DMSO), acetonitrile (MeCN), isopropyl alcohol (IPA), *n*-butyl alcohol (*n*-BuOH), ethanol (EtOH), 2-methoxyethanol (EGME), methanol (MeOH), ethylene glycol (EG), and water, the powder of CNS produced the CNS suspensions with a strong solvatochromic behavior (Figure 1b and Figures S1 and S2 (Supporting Information)).

To investigate the photophysical properties of CNS in different solvents in detail, we chose water, EtOH, and DMF as representative solvents of different polarities; the CNS suspensions in these solvents are denoted as CNS-Water, CNS-EtOH, and CNS-DMF, respectively (**Figure 2**). The UV–vis spectra of these suspensions showed two main absorption bands at approximately 330 and 500 nm. The former can be assigned to the n–π^* transition of carbon nanomaterials containing oxygen defects, e.g., epoxy and hydroxyl groups,[12] while the appearance of the band near 500 nm is uniquely observed in CNS. It has been reported that, depending on the oxidation states of surface functional groups, multitudes of surface states can be populated, resulting in an absorption tail extending beyond 400 nm.[13] Thus, this band in the visible range was attributed to the electronic transitions of various surface states in CNS.

The PL of CNS was found to strongly depend on the solvent and the excitation wavelength. Specifically, under 360 nm excitation, two emission bands at ≈430 and 550–590 nm were found in all solvents (Figures S1 and S2, Supporting Information). In water, the blue emission was dominant, whereas in the less polar EtOH and DMF, a gradual increase of the yellow-to-orange band (550–590 nm) was observed. When excited at 480 nm, the prominent PL band shows clear solvatochromism from yellow (550 nm) in DMF to orange (590 nm) in water. The yellow-to-orange band originates from the surface states because the excitation was made to selectively excite the surface states, and the position of the band (550–590 nm) was strongly affected by the solvent. Under visible-light excitation at 480 nm, the QY of CNS-DMF was found to be 20.2%, which is approximately twice that of CNS-Water (8.9%) as shown in Table S1 (Supporting Information). Moreover, we examined this interesting solvent-dependent optical property of CNS by dissolving it in water/DMF mixtures of different ratios (Figure S3, Supporting Information). Under excitation at 360 nm, the main blue band with a maximum at 430 nm in water gradually changed to distinct dual bands with peaks at 430 and 538 nm in water/DMF (1:1 mixture) and to a single band with a peak at 548 nm in neat DMF. In addition, the PL of the mixture of carbon nanoring and graphene oxide was independent of the solvent polarity, which had only blue emission under UV and visible light.

The relative intensities of the two main PL bands turned out to result from the change of lifetimes of the two bands for different solvents (Figure 2d–f). For example, Figure 2d presents the acceleration of the decay of the blue band with solvent changing from water to EtOH and to DMF; the weight-averaged lifetime decreased from 5.2 to 3.0 ns (Table S2, Supporting Information). On the other hand, the relaxation time of the yellow-to-orange band increases with the same change of solvent from 1.9 to 5.0 ns for excitation at 375 nm (Figure 2e) and from 0.8 to 4.9 ns for excitation at 450 nm (Figure 2f).

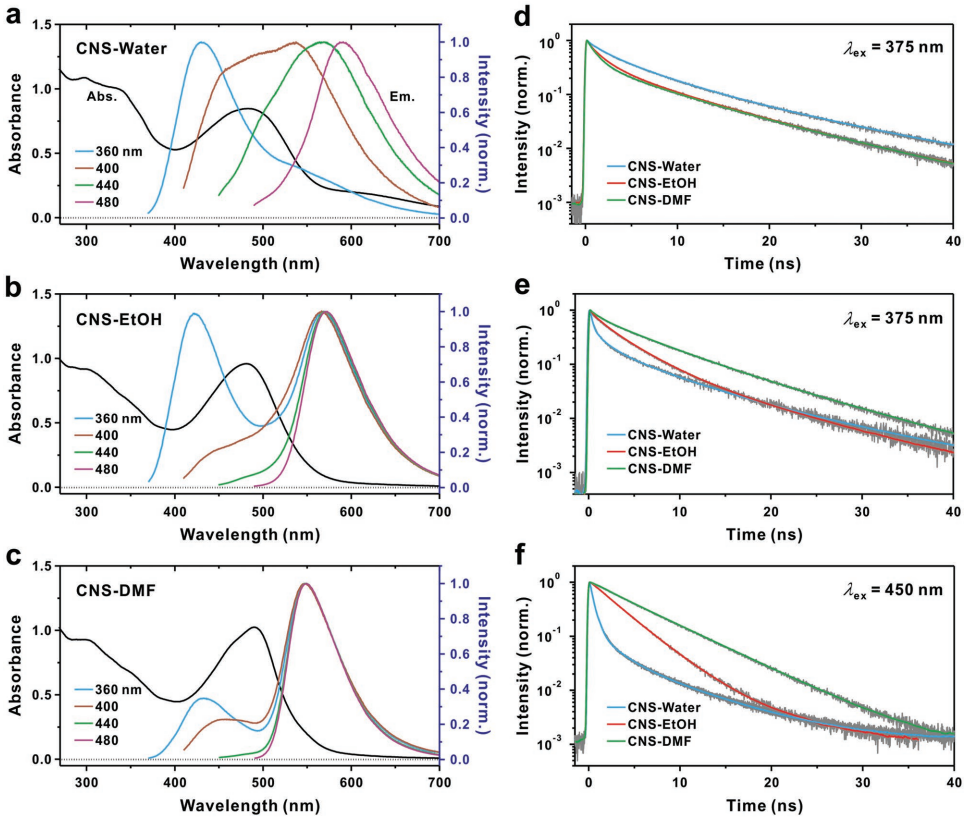

Figure 2. Photophysical properties of CNS in different solvents. a–c) UV–vis and PL spectra of CNS in (a) water, (b) ethanol (EtOH), and (c) dimethylformamide (DMF). PL spectra of CNS are given under excitation wavelengths varying from 360 to 480 nm with 40 nm increments. d–f) Normalized PL decay profiles of CNS in the three representative solvents monitored at (d) 430 nm; (e) 590 (in water), 575 (in EtOH), and 550 nm (in DMF); and (f) 590 (in water), 575 (in EtOH), and 550 nm (in DMF). The excitation wavelengths are given in each panel.

Accordingly, the shape of the steady-state PL spectrum is a consequence of the opposite time dependences of the two main bands with the same solvent series.

Transmission electron microscopy (TEM) revealed the graphene-sheet-like structure of CNS-Water with the occasional appearance of nanorings having 15 nm in diameter on it (**Figure 3**a,b). The crystalline carbon nanorings had an interlayer spacing of 0.34 nm, corresponding to the (002) interplanar spacing of graphene in the high-resolution TEM image, as reported in the literature.[14] These nanorings are proposed to originate from the carbonization of molecular precursors on graphene sheets during the hydrothermal reaction. In stark contrast, we found that the CNS-DMF existed in a folded and crumpled morphology with an average diameter of 110 ± 10 nm, suggesting their morphology transition in different solvents (Figure 3c,d). The suspension in DMF was very stable over several months without forming any noticeable aggregates. In accordance with this observation, dynamic light scattering (DLS) analysis suggested different morphologies in water and DMF with an average hydrodynamic diameter of 1280 ± 330 and 310 ± 20 nm, respectively. Although there are some deviations from the size measured using TEM in a dried state, the size of CNS was measured in a reproducible manner. In addition, the morphology of CNS depended on solvent polarity, and particularly on the properties of solvents such as hydrogen (H)-bonding (protic vs aprotic) (see other examples of TEM and DLS in Figure 3e and Figure S4 in the Supporting Information). When the solvent was exchanged from DMF to water or in reverse, reversible morphologies and spectroscopic properties were confirmed (Figure S5, Supporting Information).

To account for the shape-induced tuning of the optical properties of CNS in different solvents, we prepared a control set through the hydrothermal reaction of the small molecular precursors in the absence of GO nanosheets. The prepared carbon nanoparticles were found to exist in a carbon-nanoring-like structure with an average diameter of 20 nm and displayed consistent blue emission at ≈440 nm irrespective of solvent polarity (Figure S6, Supporting Information). Unlike CNS, this carbon nanoring did not disperse well in less polar solvents such as EtOH or DMF, whereas GO nanosheets are highly dispersible in DMF. Taken together these results, the graphitic carbon nanorings with limited solubility anchored on the surface of GO nanosheets play an important role in inducing the change of morphology.

Solubility is a consequence of physical interactions between solute and solvent molecules. To address the molecular interactions, the elucidation of the chemical composition of CNS is a prerequisite. To this end, FT-IR and XPS were employed. The FT-IR spectrum of CNS-Water revealed oxygen functional groups such as COOH at 1677 cm^{-1} with a broad peak corresponding to O—H and N—H stretching at 3222 cm^{-1} (Figure S7, Supporting Information). Interestingly,

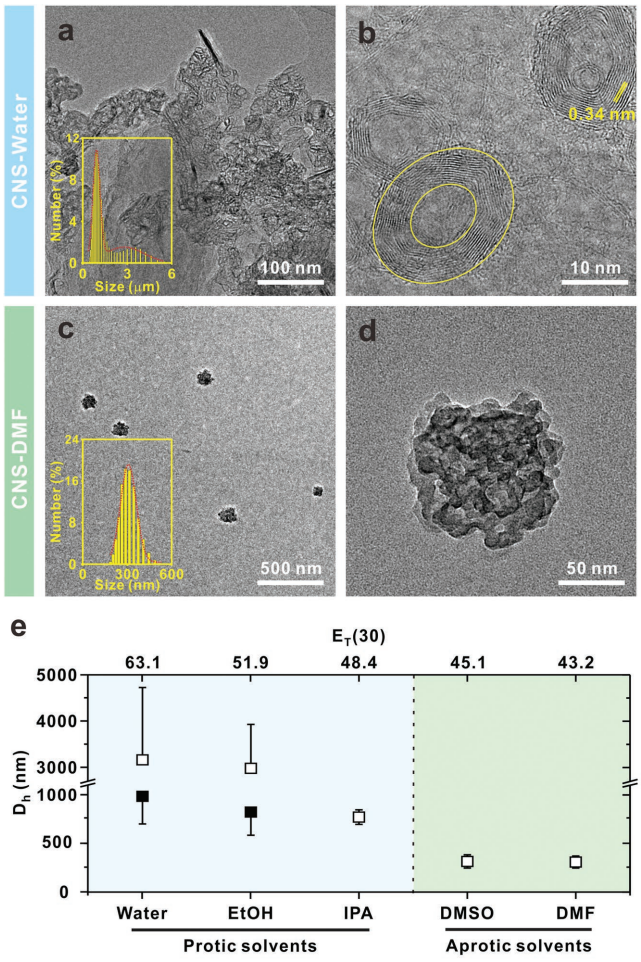

Figure 3. Morphology transformation of CNS in different solvents. a–d) TEM images of (a, b) CNS-Water and (c, d) CNS-DMF. Note that the TEM samples were prepared after drying off each solvent. Insets in (a) and (c) show the size-distribution histograms of CNS-Water and CNS-DMF measured by DLS, respectively. e) Hydrodynamic diameter (D_h) of CNS in different solvents measured by DLS with a volume-averaged fraction of major (open) and minor (closed) components ($n = 10$).

in CNS-DMF, sp^3-domain-related peaks at 2851 and 2927 cm^{-1} were dominant. In accordance with the FT-IR results, the deconvoluted high-resolution C1s XPS spectrum of CNS-Water displayed a high content (≈22%) of oxygen groups such as hydroxyl, carbonyl, and carboxylic groups, whereas these groups decreased significantly to ≈5% in CNS-DMF (Figure S8 and Table S3, Supporting Information). In addition, the ratio of sp^2- and sp^3-domains in C1s changed from 1.14 to 0.28 upon solvent change from water to DMF. Considering the facts that the probing depth of XPS is several nanometers at most and the chemical compositions determined from the XPS can be reversibly reproduced upon switching the solvent, the reduction of the fraction of oxygen-related functional groups in DMF under the XPS measurements indicates that CNS-DMF folded in a way that the exposure of the oxygen-related surface groups is minimized. The results from the XPS measurements match the TEM and the DLS results well.

Based on the chemical structure of CNS discussed above, the nature of the solute–solvent interaction (i.e., solvation) can be discussed at a molecular level. Solvation comprises nonspecific and specific interactions, which result from the dipolarity/polarizability and H-bonding capability of a solvent, respectively.[15] While the $E_T(30)$ index of solvents is commonly used to represent the polarity of solvents, the value is obtained from the phenomenological solvatochromism of a dye in a series of solvents.[16] On the other hand, the Kamlet–Taft (K–T) parameters α, β, and π^* allow for the categorization of the specific and nonspecific solvation properties of solvents.[17] The α and β scales of a solvent describe the ability of the solvent to donate and accept a H-bond, respectively, while π^* is a measure of the ability of a solvent to stabilize a charge/dipole with its dielectric effect. Among these parameters, the plot against the K–T acidity parameter, α, of solvents shows a significant correlation, as depicted in **Figure 4**a and Figure S9 (Supporting Information). As observed in the solvent-dependent PL lifetime of the green-to-orange band from 4.9 ns (CNS-DMF) to 2.8 ns (CNS-EtOH) and to 760 ps (CNS-Water) (Figure 2), this dynamic trend is in accordance with the common reduction of the excited-state lifetime of organic dyes having H-bond-accepting oxygen-related groups in protic solvents; when the interaction between electron-withdrawing groups and protic solvent molecules becomes stronger, the fluorescence lifetime decreased owing to H-bond-assisted nonradiative deactivation.[18] It has recently been reported that carbon nanomaterials displayed a similar trend as well.[19] Overall, the H-bonding between the nonbonding electrons of oxygen-related surface groups and the protic hydrogen of a solvent molecule is crucial in the solvation of CNS.

Considering the solvatochromism and morphological tunability of CNS with respect to solvents, the following mechanistic framework for the morphology-induced solvatochromism can be rationalized. First, the specific solvation of CNS via H-bonding by protic solvent molecules is key for the reversible folding/unfolding morphological transformation of CNS (Figure 4b). In protic solvents, nonbonding electrons of the oxygen-related functional groups of CNS can be effectively stabilized via the formation of H-bonds with protic hydrogen atoms of the solvent. However, in aprotic solvents, the deficiency of such preferential interaction causes the CNS to search for another option of the lowest free energy. This alternative can be achieved if the CNS folds in a crumpled morphology so that the exposure of the electronegative oxygen atoms to the aprotic environment becomes minimal, while the number of intra-CNS H-bonds among oxygen-related surface functional groups is maximized.

Second, the tunability of the steady-state PL of CNS with its morphology originates from the reversal of the lifetimes of the two main PL bands (Figure 4c). When CNS is unfolded in a flat morphology, the oxygen-related functional groups are H-bonded to protic solvent molecules. This leads to the acceleration of the nonradiative transition of the surface states so that the green-to-orange band emitting from the GO nanosheet has a relatively shorter excited-state lifetime than that of the blue band originating from the carbon nanoring islands. Once the CNS folds into a crumpled, crowded conformation, the lifetime of the green-to-orange band increases because of the lack of efficient

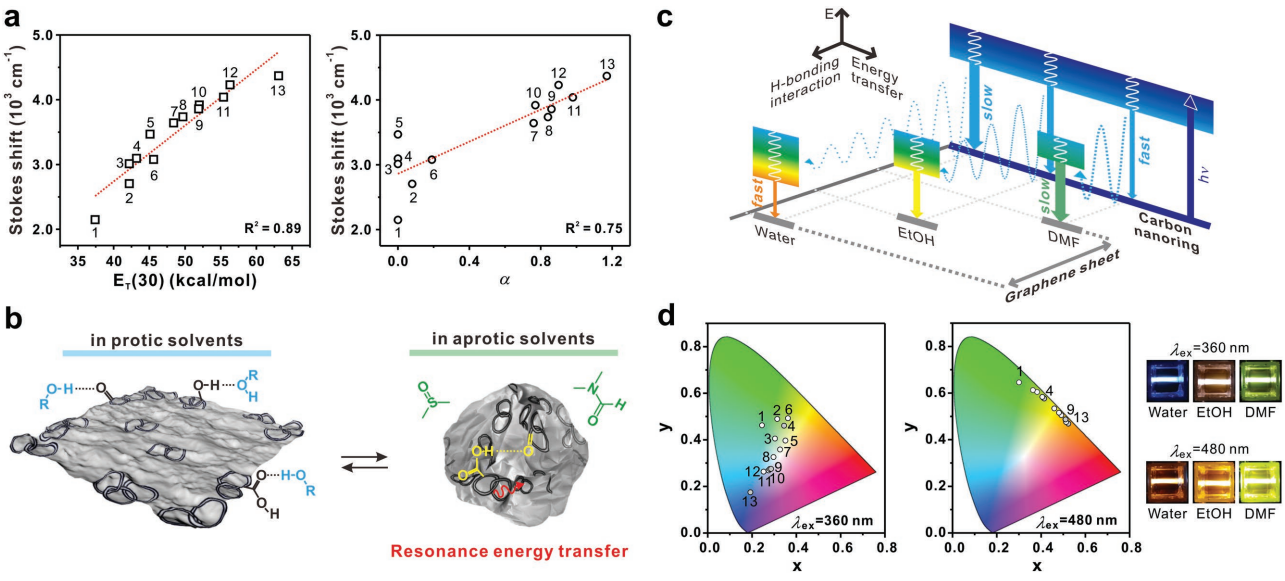

Figure 4. Solvatochromic properties of CNS. a) Stokes shifts of the yellow-to-orange PL band with excitation at 480 nm, as a function of solvent polarity factor, E_T(30), and a Kamlet–Taft acidity parameter (α). b) Schematic representation of the changeable morphology of CNS in protic and aprotic solvents. c) Proposed energy diagram of CNS in different solvents. d) CIE coordinates calculated from the PL spectra of solvents with different polarities under excitation at 360 nm (left) and 480 nm (right). Optical images of CNS suspension in each solvent under excitation at (top) 360 nm and (bottom) 480 nm. Solvents used in CIE coordinates are as follows. 1: THF, 2: Acetone, 3: NMP, 4: DMF, 5: DMSO, 6: ACN, 7: IPA, 8: *n*-BuOH, 9: EtOH, 10: EGME, 11: MeOH, 12: EG, 13: Water. See the text for acronyms of the solvents.

vibrational relaxation to solvent molecules. In turn, the folding of CNS is proposed to open a relaxation channel for the blue emission of carbon nanorings via resonance energy transfer to a distribution of adjacent surface domains of GO nanosheets, which absorb the blue-region emission in the crowded morphology; the weight-averaged lifetime of the blue PL band decreases in aprotic solvents compared to that in protic solvents, e.g., from 5.2 ns for CNS-Water to 3.0 ns for CNS-DMF. The efficiency (E) of the resonance energy transfer is closely related to the distance between the energy donor and acceptor, modulating the lifetime of the donor according to the following relationship: $E = 1 - \tau_F/\tau_D$, where τ_D is the fixed PL lifetime of the donor and τ_F is the shortened lifetime resulting from the resonance energy transfer.[20] Here, τ_F was obtained by the weighted average of multiexponential decay components of the PL of CNS, while τ_D was taken from the PL lifetime of ring-shaped carbon islands without sheet-like support in water (Table S4, Supporting Information). Accordingly, the efficiencies of the resonance energy transfer were estimated to be 0.1, 0.4, and 0.5 in water, EtOH, and DMF, respectively. We suggest that mechanism of color tuning is the balance between the steady-state intensities of the two main PL bands of CNS achieved by modulating their lifetimes and preferential excited-state population with the choice of solvent and excitation wavelength, respectively.

Finally, CIE coordinates indicate that the PL emission of CNS is significantly influenced by the solvent. Various emission colors that were widely scattered in the CIE coordinate were observed with excitation at 360 nm for different solvents (Figure 4d). It worth noting that, among the various solvents tested, the CIE coordinate of CNS dispersed in IPA (0.30, 0.33) is very close to that of white light (0.33, 0.33), indicating high potential for optoelectronic applications.

In conclusion, we developed solvatochromic carbon nanosheets through the carbonization of small molecular precursors in the presence of GO nanosheets as a template. Owing to the abundant surface oxygen groups and clusters of carbon nanorings, excitation-dependent behavior was observed in CNS-Water. Upon switching to DMF, an aprotic solvent, the folded and crumpled structure of CNS showed green emission owing to the maximized H-bonding within a CNS, as evidenced from structural and photophysical analyses such as XPS, FT-IR spectroscopy, and time-correlated single-photon counting. This unique design of hybrid carbon nanostructures is envisioned to synergistically offer unprecedented properties, providing diverse opportunities in tailoring the optical properties of carbon nanomaterials. We anticipate that this solvatochromic CNS poses promising opportunities in optoelectronic devices and sensors.

Experimental Section

Preparation of GO Nanosheet: GO was synthesized from graphite powder (45 µm, Baycarbon) by modified Hummers method and exfoliated to give a brown dispersion of graphene oxide under ultrasonication.[21]

Synthesis of Solvatochromic CNSs: All materials were purchased from Sigma-Aldrich. To prepare CNS, 96 mg of citric acid (0.50 mmol, $C_6H_8O_7$), 31 mg of boric acid (0.50 mmol, H_3BO_3), and 34.7 µL of ethylenediamine (0.50 mmol, $C_2H_8N_2$) were added to 10 mL of 0.50 mg mL^{-1} GO. After stirring for 10 min, the aggregated black solution was placed into a Teflon-lined stainless steel autoclave. After hydrothermal reaction at 180 °C for 6 h, a dark-brown solution (supernatant) and black powder (precipitate) were produced through carbonization. The precipitate was washed five times with 6 mL of ethanol and chloroform (1:1 v/v) through the centrifugation and the supernatant was discarded (5 mL each). In

this step, small carbon nanostructures with highly blue-fluorescing molecular chromophores without exhibiting solvatochromism were discarded in the supernatant. Then, the final supernatant (6 mL) having a green-yellow emission was collected through the centrifugation and evaporated in vacuum to give a final CNS powder (typical isolated yield of 2%–3% from the mass of precursors). Finally, the resulting powder was dissolved in each solvent at a concentration of 0.50 mg mL^{-1}. The small molecules were carbonized under identical conditions in the absence of GO.

Characterization: A UV–vis spectrophotometer (UV-2550, Shimadzu) was used to obtain the absorption spectra of CNS. A fluorimeter (RF-6000, Shimadzu) was used to measure the emission spectra of CNS. The structure of the CNS was analyzed using XPS (K-alpha, Thermo Fisher) and FT-IR spectroscopy (Cary 660, Varian). The morphology and size of CNSs were measured using a transmission electron microscope (JEM-2100, JEOL). Fluorescence lifetimes were measured using a time-correlated single photon counting spectrometer (Fluotime 300, PicoQuant) with the light sources of picosecond-pulsed diode lasers, emitting at 375 nm (LDH-D-C-375, PicoQuant) and 450 nm (LDH-D-C-450, PicoQuant). The total instrument response function was 200–220 ps. All PL decay profiles were fitted to multiple-exponential functions by using software (FluoFit, PicoQuant) to deduce PL lifetimes.

Supporting Information

Supporting Information is available from the Wiley Online Library or from the author.

Acknowledgements

This work was supported by the National Research Foundation of Korea (NRF) grant (NRF-2014R1A2A1A11052829, 2015R1A2A2A04003160, and 2014R1A1A1008289) and by the Institute of Basic Science (IBS-R020-D1), Korea.

Conflict of Interest

The authors declare no conflict of interest.

Keywords

carbon nanomaterials, hydrogen bonding, morphology, photoluminescence, solvatochromism

Received: February 23, 2017
Revised: March 13, 2017
Published online: April 18, 2017

[1] a) L. Cao, M. J. Meziani, S. Sahu, Y. P. Sun, *Acc. Chem. Res.* **2013**, *46*, 171; b) O. Kozak, M. Sudolská, G. Pramanik, P. Cigler, M. Otyepka, R. Zboril, *Chem. Mater.* **2016**, *28*, 4085.

[2] a) F. Liu, M. H. Jang, H. D. Ha, J. H. Kim, Y. H. Cho, T. S. Seo, *Adv. Mater.* **2013**, *25*, 3657; b) C. T. Chien, S. S. Li, W. J. Lai, Y. C. Yeh, H. A. Chen, I. S. Chen, L. C. Chen, K. H. Chen, T. Nemoto, S. Isoda, M. W. Chen, T. Fujita, G. Eda, H. Yamaguchi, M. Chhowalla, C. W. Chen, *Angew. Chem., Int. Ed.* **2012**, *51*, 6662; c) Y. P. Sun, B. Zhou, Y. Lin, W. Wang, K. A. S. Fernando, P. Pathak, M. J. Meziani, B. A. Harruff, X. Wang, H. F. Wang, P. J. G. Luo, H. Yang, M. E. Kose, B. L. Chen, L. M. Veca, S. Y. Xie, *J. Am. Chem. Soc.* **2006**, *128*, 7756.

[3] S. N. Baker, G. A. Baker, *Angew. Chem., Int. Ed.* **2010**, *49*, 6726.

[4] a) H. Ding, S. B. Yu, J. S. Wei, H. M. Xiong, *ACS Nano* **2016**, *10*, 484; b) S. Hu, A. Trinchi, P. Atkin, I. Cole, *Angew. Chem., Int. Ed.* **2015**, *54*, 2970; c) K. Jiang, S. Sun, L. Zhang, Y. Lu, A. Wu, C. Cai, H. Lin, *Angew. Chem., Int. Ed.* **2015**, *54*, 5360; d) H. Tetsuka, A. Nagoya, T. Fukusumi, T. Matsui, *Adv. Mater.* **2016**, *28*, 4632.

[5] a) Z.-Z. Lu, R. Zhang, Y.-Z. Li, Z.-J. Guo, H.-G. Zheng, *J. Am. Chem. Soc.* **2011**, *133*, 4172; b) X. Yan, T. R. Cook, P. Wang, F. Huang, P. J. Stang, *Nat. Chem.* **2015**, *7*, 342; c) J. Lee, H. T. Chang, H. An, S. Ahn, J. Shim, J.-M. Kim, *Nat. Commun.* **2013**, *4*, 2641.

[6] a) S. J. Zhu, J. H. Zhang, C. Y. Qiao, S. J. Tang, Y. F. Li, W. J. Yuan, B. Li, L. Tian, F. Liu, R. Hu, H. N. Gao, H. T. Wei, H. Zhang, H. C. Sun, B. Yang, *Chem. Commun.* **2011**, *47*, 6858; b) S. K. Cushing, M. Li, F. Q. Huang, N. Q. Wu, *ACS Nano* **2014**, *8*, 1002; c) Y. Chen, M. Zheng, Y. Xiao, H. Dong, H. Zhang, J. Zhuang, H. Hu, B. Lei, Y. Liu, *Adv. Mater.* **2016**, *28*, 312; d) O. Kozák, K. K. R. Datta, M. Greplová, V. C. Ranc, J. Kašlík, R. Zbořl, *J. Phys. Chem. C* **2013**, *117*, 24991.

[7] a) H. Wang, C. Sun, X. Chen, Y. Zhang, V. L. Colvin, Q. Rice, J. Seo, S. Feng, S. Wang, W. Y. William, *Nanoscale* **2017**, *9*, 1909; b) A. Sciortino, E. Marino, B. van Dam, P. Schall, M. Cannas, F. Messina, *J. Phys. Chem. Lett.* **2016**, *7*, 3419.

[8] X. Zheng, J. Luo, W. Lv, D. W. Wang, Q. H. Yang, *Adv. Mater.* **2015**, *27*, 5388.

[9] a) X. D. Zhuang, F. Zhang, D. Q. Wu, X. L. Feng, *Adv. Mater.* **2014**, *26*, 3081; b) T. T. Xie, W. Lv, W. Wei, Z. J. Li, B. H. Li, F. Y. Kang, Q. H. Yang, *Chem. Commun.* **2013**, *49*, 10427.

[10] D. Krishnan, K. Raidongia, J. Shao, J. Huang, *ACS Nano* **2013**, *8*, 449.

[11] Y. Choi, B. Kang, J. Lee, S. Kim, G. T. Kim, H. Kang, B. R. Lee, H. Kim, S.-H. Shim, G. Lee, O.-H. Kwon, B.-S. Kim, *Chem. Mater.* **2016**, *28*, 6840.

[12] Y. Wang, S. Kalytchuk, Y. Zhang, H. C. Shi, S. V. Kershaw, A. L. Rogach, *J. Phys. Chem. Lett.* **2014**, *5*, 1412.

[13] S. K. Das, Y. Y. Liu, S. Yeom, D. Y. Kim, C. I. Richards, *Nano Lett.* **2014**, *14*, 620.

[14] X. Li, Y. Liu, X. Song, H. Wang, H. Gu, H. Zeng, *Angew. Chem., Int. Ed.* **2015**, *54*, 1759.

[15] O. F. Mohammed, O.-H. Kwon, C. M. Othon, A. H. Zewail, *Angew. Chem., Int. Ed.* **2009**, *48*, 6251.

[16] V. G. Machado, R. I. Stock, C. Reichardt, *Chem. Rev.* **2014**, *114*, 10429.

[17] J. M. Lee, S. Ruckes, J. M. Prausnitz, *J. Phys. Chem. B* **2008**, *112*, 1473.

[18] P. Fita, M. Fedoseeva, E. Vauthey, *J. Phys. Chem. A* **2011**, *115*, 2465.

[19] D. Ghosh, G. Ahamed, S. Batuta, N. A. Begum, D. Mandal, *J. Phys. Chem. A* **2016**, *120*, 44.

[20] a) H. F. Dong, W. C. Gao, F. Yan, H. X. Ji, H. X. Ju, *Anal. Chem.* **2010**, *82*, 5511; b) E. Morales-Narvaez, B. Perez-Lopez, L. B. Pires, A. Merkoci, *Carbon* **2012**, *50*, 2987.

[21] Y. Choi, M. Gu, J. Park, H. K. Song, B.-S. Kim, *Adv. Energy Mater.* **2012**, *2*, 1510.

